

## Ultrafast Transport of Laser-Excited Spin-Polarized Carriers in Au/Fe/MgO(001)

Alexey Melnikov,<sup>1,2,\*</sup> Ilya Razdolski,<sup>3,†</sup> Tim O. Wehling,<sup>4</sup> Evangelos Th. Papaioannou,<sup>2,‡</sup> Vladimir Roddatis,<sup>5</sup>  
Paul Fumagalli,<sup>2</sup> Oleg Aktsipetrov,<sup>3</sup> Alexander I. Lichtenstein,<sup>4</sup> and Uwe Bovensiepen<sup>2,6</sup>

<sup>1</sup>Physical Chemistry Department, Fritz-Haber-Institute of the Max Planck Society, Faradayweg 4-6, 14195 Berlin, Germany

<sup>2</sup>Physics Department, Freie Universität Berlin, Arnimallee 14, 14195 Berlin, Germany

<sup>3</sup>Physics Department, Moscow State University, 119991 Moscow, Russia

<sup>4</sup>Theoretical Physics Institute, University of Hamburg, Jungiusstrasse 9, 20355 Hamburg, Germany

<sup>5</sup>NRC “Kurchatov Institute,” place Akademika Kurchatova 1, Moscow, 123182, Russia

<sup>6</sup>Faculty of Physics, University of Duisburg-Essen, Lotharstrasse 1, 47048 Duisburg, Germany

(Received 4 March 2011; published 12 August 2011)

Hot carrier-induced spin dynamics is analyzed in epitaxial Au/Fe/MgO(001) by a time domain approach. We excite a spin current pulse in Fe by 35 fs laser pulses. The transient spin polarization, which is probed at the Au surface by optical second harmonic generation, changes its sign after a few hundred femtoseconds. This is explained by a competition of ballistic and diffusive propagation considering energy-dependent hot carrier relaxation rates. In addition, we observe the decay of the spin polarization within 1 ps, which is associated with the hot carrier spin relaxation time in Au.

DOI: 10.1103/PhysRevLett.107.076601

PACS numbers: 72.25.Ba, 72.25.Fe, 73.23.Ad, 78.47.J–

The quest for fast, high-density, nonvolatile magnetic memory is a key motivation for research in the field of spin dynamics in low-dimensional ferromagnetic structures. In recent years, magnetization dynamics has seen a remarkable development from classical precession on the nanosecond scale to the ultrafast regime accessible by femtosecond laser pulses [1]. These findings still challenge the understanding of ultrafast magnetism, and insight into the underlying elementary processes even in simple systems like Fe, Co, and Ni is just at the beginning: (i) Koopmans and co-workers consider spin-lattice interaction as one origin of femtomagnetism and have developed an empirical model based on spin-orbit mediated electron spin-flip scattering [2,3]; (ii) Bigot, Vomir, and Beaurepaire [4] and Zhang *et al.* [5] suggest that the light field is directly involved in magnetization dynamics; (iii) Battiato, Carva, and Oppeneer propose superdiffusive spin transport being responsible for the ultrafast demagnetization [6], which couples the fields of ultrafast spin dynamics and stationary spin transport [7]. It was shown [8] that in spin valve structures spin-polarized carrier transport speeds up and enhances the demagnetization compared to single ferromagnetic layers. Without a doubt, there is a need for further investigations and development of a profound microscopic understanding. Novel experimental approaches, like the one presented here, bear the chance to overcome limitations of established schemes, which have difficulties to separate photon-, electron-, and phonon-mediated effects on the magnetization under non-equilibrium conditions established after femtosecond laser excitation.

Our experimental approach is based on the front-pump–back-probe scheme used for the investigations of hot carrier (HC) dynamics in gold [9,10]: HCs were excited by a

short laser pulse within the optical skin depth  $\lambda_{\text{Au}}^S \approx 15$  nm at the front side of a thin Au film. The transient reflectivity  $\Delta R/R$  monitoring HCs traversing the film was measured at the back side through a transparent substrate. The delay in the onset of  $\Delta R/R$  gives a direct measure of the HC propagation velocity.

To make the excited HCs spin-polarized, we introduce a thin film of ferromagnetic metal (Fe) of thickness  $d_{\text{Fe}} \approx \lambda_{\text{Fe}}^S$  as shown in Fig. 1, inset. The pump laser pulse focused onto the sample from the back (substrate) side excites HCs

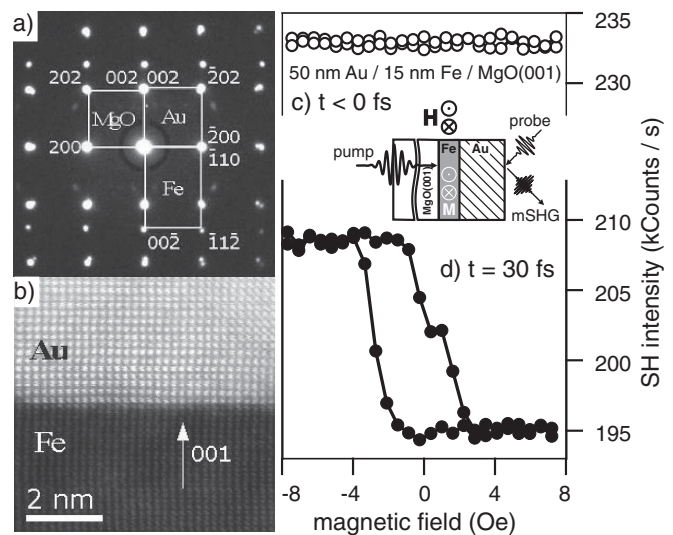


FIG. 1. Electron diffraction pattern of Au/Fe/MgO(001) (a), dark field scanning transmission electron microscope image of the Fe/Au interface (b), and SH hysteresis loops at the Au surface before (c) and after (d) the excitation. The inset illustrates the pump-probe experiment.

in the exchange-split band structure of Fe. Traversing the Au film, these HCs may carry the spin polarization (SP) forming a pulse of spin current (SC). Since no bias voltage is applied, the charge component of this current might be screened by a displacement of “cold” carriers in Au on the subfemtosecond time scale of inverse plasma frequency [11]. This makes a dramatic difference to spin-polarized electric currents used for the spin transfer in spintronics [12]: There the lateral size of devices is limited to 10–100 nm due to the charge current inducing the Oersted field proportional to the area of the device. Our approach has the potential to overcome such limitations. The SC pulse is detected at the Au surface by a magneto-optical signal from the probe laser pulse focused onto the sample from the front (Au) side. If  $d_{\text{Au}} \gg \lambda_{\text{Au}}^S$ , this signal is sensitive neither to the electromagnetic field of the pump pulse nor to the lattice excitations induced by the pump absorption since the sound velocity is 3 orders of magnitude slower than the HC propagation.

In this Letter, we prove the possibility of separation of ballistic and diffusive contributions to SC directly in the time domain. A femtosecond experiment in a back-pump–front-probe configuration on a Fe(001)/Au(001) layer stack is employed to realize a time-of-flight-like approach with magneto-optical detection.

Thin films of Fe(001) and Au(001) are grown following [13,14] on optically transparent MgO(001) and examined with the scanning transmission electron microscope TITAN 80-300 (FEI, USA) equipped with a spherical aberration corrector and a high angle annular dark field detector. The films grow epitaxially [Figs. 1(a) and 1(b)] with  $[001]_{\text{Au}} \parallel [001]_{\text{Fe}} \parallel [001]_{\text{MgO}}$  and  $[010]_{\text{Au}} \parallel [110]_{\text{Fe}} \parallel [010]_{\text{MgO}}$  [15]. The Fe film is magnetized in-plane with the help of an electromagnet.

Second harmonic (SH) generation is used in a back-pump–front-probe scheme for the surface SP detection. The  $p$ -polarized 35 fs, 800 nm, 40 nJ/pulse, 1.52 MHz output of a cavity dumped Ti:sapphire oscillator is split at a power ratio of 4:1 into pump and probe pulses. The pump is chopped with a frequency of 500 Hz, and the intensity of the  $p$ -polarized SH from the probe is recorded by a two-channel photon counter. The pump-probe delay  $t = 0$  is defined at a region with  $d_{\text{Au}} = 2$  nm on each sample, by the maximum of noncollinear SH in the direction between transmitted pump and reflected probe beams. The electric field at SH  $\vec{E}(2\omega) = \vec{E}_{\text{even}}(2\omega) + \vec{E}_{\text{odd}}(2\omega)$  consists of even and odd terms with respect to the reversal of the magnetization  $\vec{M}$  [16]:  $\vec{E}_{\text{even}}$  is independent of  $\vec{M}$  and  $\vec{E}_{\text{odd}} = \vec{\alpha}M$ , where  $M$  is the projection of  $\vec{M}$  perpendicular to the optical plane of incidence in the case of  $p$ -in,  $p$ -out geometry. Although SC can generate a sizable bulk dipole magneto-induced SH term in semiconductors [17,18], in metals only the dipole-allowed surface SH is expected owing to the small  $\lambda^S$ . Thus, here  $\vec{M}$  is associated with the SP induced by HCs at the Au surface.

The surface SP is monitored by the SH intensity

$$I(2\omega) \propto |\vec{E}_{\text{even}}(2\omega) + \vec{E}_{\text{odd}}(2\omega)|^2 \approx kM + c \quad (1)$$

for  $E_{\text{even}} \gg E_{\text{odd}}$  with  $c \equiv E_{\text{even}}^2$  and  $k \equiv 2\vec{\alpha}\vec{E}_{\text{even}}$ . At  $t < 0$ ,  $I(2\omega)$  is independent of the external magnetic field  $H$  applied perpendicular to the plane of incidence [Fig. 1(c)], as is expected for the nonperturbed surface of a paramagnetic metal. However, shortly after the excitation, a dependence  $I(H)$  is observed [Fig. 1(d)], which closely resembles the hysteresis loop measured at the Fe/MgO interface with the back probe: HCs imprint the hysteresis loop of Fe onto the Au surface.

To study the surface dynamics in more details, the SH intensity is measured vs  $t$  in the saturating  $H$  of opposite polarities with  $[I^{\uparrow}(t)]$  and without ( $I_0^{\uparrow}$ ) the excitation. The electronic response is characterized by

$$\Delta(t) \equiv \frac{E_{\text{even}}(t) - E_{\text{even}}^0}{E_{\text{even}}^0} = \sqrt{\frac{I^{\uparrow}(t) + I^{\downarrow}(t)}{I_0^{\uparrow} + I_0^{\downarrow}}} - 1, \quad (2)$$

and the transient SP by the SH magnetic contrast

$$\rho(t) = \frac{I^{\uparrow}(t) - I^{\downarrow}(t)}{I^{\uparrow}(t) + I^{\downarrow}(t)} = \frac{k(t)M(t)}{c(t)} \propto M(t). \quad (3)$$

Hot electrons (holes) reaching the Au surface increase (reduce) the population of states above (below) the Fermi level, which are involved in the SH generation process as unoccupied intermediate (occupied initial) states. Thereby, HCs should reduce the SH yield (equally both  $E_{\text{even}}$  and  $E_{\text{odd}}$ ) leading to a negative  $\Delta(t)$  independently of their type and SP. These effects, however, cancel each other in the nominator and denominator of Eq. (3), so that  $\rho(t)$  monitors only the SP created by HCs at the surface.

Typical results are presented in Figs. 2(a)–2(d). At the surface of 50 nm Au(001),  $\Delta(t)$  establishes an ultrafast drop and recovery on time scales of 50 fs and 1 ps, respectively. The first one can be characterized by the center  $\tau_c \approx 10$  fs and the width  $\tau_f \approx 70$  fs of the negative front of  $\Delta(t)$  [Fig. 2(a)]. In the case of  $d_{\text{Au}} = 100$  nm, the front shifts to  $\tau'_c \approx 70$  fs and broadens to  $\tau'_f \approx 200$  fs; the recovery is also delayed [Fig. 2(b)]. After the excitation, the surface SP builds up and reaches its maximal value at 40 (80) fs for  $d_{\text{Au}} = 50$  (100) nm [Fig. 2(c)]. The 40 fs delay agrees with the time required for the traversing of 50 nm of Au by HCs propagating with velocities  $v_{\text{Au}}^{\text{HC}}$  close to the Fermi velocity  $v_{\text{Au}}^F \approx 1.4$  nm/fs [9], which is a signature of ballistic HC transport. Later on,  $\rho(t)$  changes the sign, establishes a second extremum at 0.35 (0.5) ps, and relaxes to  $\rho = 0$  at 1.2 ps for both  $d_{\text{Au}}$  [Fig. 2(d)]. To explain this,  $v_{\text{Au}}^{\text{HC}} \ll v_{\text{Au}}^F$  is considered, which originates from scattering of a fraction of HCs leading to diffusive transport. It has been shown [9,10,19] that the HC transport is almost purely ballistic for  $d_{\text{Au}} < 100$  nm; for thicker films, a significant diffusive component appears and increases with  $d_{\text{Au}}$ . Note that the thickness dependence of the

ballistic-to-diffusion transport ratio will be affected by the energy spectrum of HCs which is different for the HC excitation in Au and injection from Fe.

After interaction with the surface, HCs are removed from the subsurface region probed by the SH generation. This occurs via quasielastic (reflection) or inelastic scattering after which HCs move ballistically or diffuse to the Au bulk. In this picture,  $\Delta(t)$  monitors the time profile of a HC packet reaching the Au surface with (i) a steep “ballistic” front and (ii) a “diffusive” slope stretched by the carrier scattering. With increasing  $d_{\text{Au}}$ , both the front and the slope become longer [Figs. 2(a) and 2(b)] due to a linear and nonlinear increase of the time of flight of ballistic and diffusive HCs, respectively. In addition, the ballistic HC fraction is reduced, because the ballistic propagation length  $\lambda_{\text{Au}}^{\text{HC}}$  is comparable to  $d_{\text{Au}}$  and a longer propagation increases the scattering probability.

The magnetic contrast  $\rho$  is proportional to the SP transferred to the Au surface by two groups of HCs excited in Fe: (i)  $\text{HC}^+$ , majority electrons  $e^\uparrow$  and minority holes  $h^\downarrow$  carrying positive SP, and (ii)  $\text{HC}^-$ ,  $e^\downarrow$  and  $h^\uparrow$  with negative SP. The observed nonmonotonic behavior of  $\rho(t)$  can be explained by a diffusive fraction of  $\text{HC}^+$  which is larger than that of  $\text{HC}^-$ . Then the leading edge of the HC packet will be formed predominantly by  $\text{HC}^-$ , while  $\text{HC}^+$  will dominate at the trailing part providing the sign change of  $\rho(t)$  [Fig. 2(c)]. The spin dependence  $\lambda_{\text{Au}}^{\text{HC}^+} < \lambda_{\text{Au}}^{\text{HC}^-}$  in the paramagnetic Au originates from the dependence of  $v_{\text{Au}}^{\text{HC}}$  and the HC lifetime  $\tau_{\text{Au}}^{\text{HC}}$  on the HC energy  $\epsilon^{\text{HC}}$ : The ballistic length  $\lambda_{\text{Au}}^{\text{HC}} = v_{\text{Au}}^{\text{HC}} \cdot \tau_{\text{Au}}^{\text{HC}}$  depends on  $\epsilon^{\text{HC}}$ , which

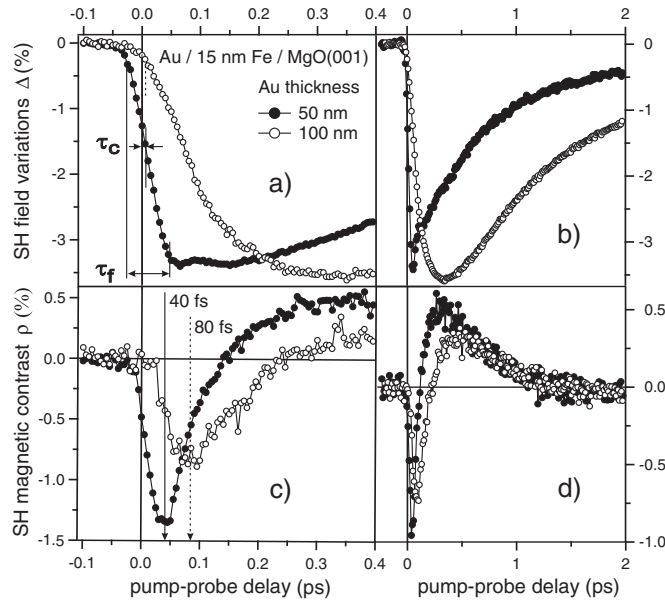


FIG. 2. Pump-induced variation of SH electronic contribution  $\Delta$  (a),(b) and SH magnetic contrast  $\rho \propto M$  (c),(d) measured at the Au surface of the Au/Fe/MgO(001) structure with the indicated  $d_{\text{Fe}}$  and  $d_{\text{Au}}$  for the pump fluence of  $1 \text{ mJ/cm}^2$ .

is connected to the HC spin orientation due to excitation conditions in Fe.

To optimize these spin-dependent propagation effects,  $d_{\text{Fe}}$  should be large enough to excite HCs mostly in Fe but not in Au and small enough to keep the larger ballistic fraction. Since  $\lambda_{\text{Fe}}^{\text{HC}} \sim \lambda_{\text{Fe}}^{\text{S}}$ , the leading part of the spin-polarized HC packet generated in Fe is preceded by some non-spin-polarized HCs generated in Au, which leads to an earlier onset of  $\Delta(t)$  compared to  $\rho(t)$  [Figs. 2(a) and 2(c)].

In contrast to the change of SC polarity, the duration of the overall SC pulse is determined by the decay of SP in Au:  $\rho(t) \approx 0$  after 1.2 ps [Fig. 2(d)], while  $\Delta(t) \neq 0$  [Fig. 2(b)]. Interestingly, this decay proceeds independently of the Au thickness [Fig. 2(d)]; i.e., the HCs lose their SP while they propagate through Au in the diffusive regime. In an earlier time-resolved magneto-optical study, Elezzabi, Freeman, and Johnson [20] reported the response time for the magnetic field-induced magnetization of Au  $\tau_{\text{Au}}^M \approx 45 \text{ ps}$ . The obvious difference between Ref. [20] and the present study is the SP generation process. In Ref. [20], the SP builds up under quasiequilibrium conditions, and the perturbation is an external magnetic field. In our case, the electron subsystem is in a nonequilibrium state characterized by a high density of traveling HCs (see estimations below). We explain the difference between  $\tau_{\text{Au}}^M \approx 45 \text{ ps}$  and the HC spin relaxation time  $\tau_{\text{Au}}^S \approx 1 \text{ ps}$ , observed here, by an increase of the scattering phase space for the nonequilibrium state, which includes spin-flip events.

To verify the explanation of propagation effects, the energy and momentum distribution of HCs excited in Fe was calculated based on density functional theory as implemented in the WIEN2K package [21] using the linearized augmented plane wave method and a generalized gradient approximation [22] to the exchange and correlation potential. Figure 3 shows the HC spectrum after the momentum averaging. Upon the injection of HCs across the interface,

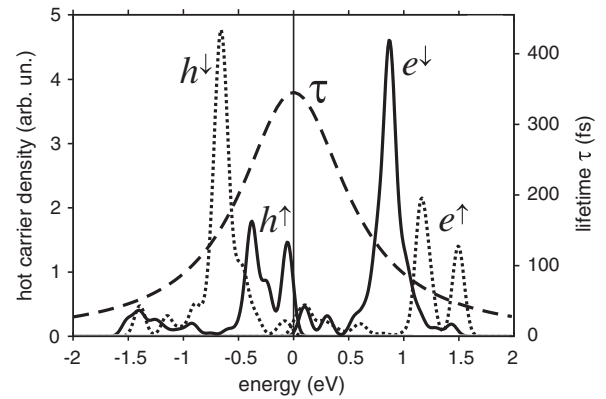


FIG. 3. Calculated density of carriers excited in Fe vs their energy with respect to the Fermi level: Solid (dotted) curves correspond to HCs carrying negative (positive) SP. The dashed curve reproduces the HC lifetime from Ref. [26].

TABLE I. Average lifetimes  $\tau$ , ballistic velocities  $v$ , and ballistic lengths  $\lambda = v\tau$  in Au for different types of spin-polarized hot carriers excited in Fe by an 800 nm laser pulse and injected into Au through the Fe/Au interface.

	$v$ , nm/fs	$\tau$ , fs	$\lambda$ , nm
$e^\uparrow$	0.95	60	57
$h^\downarrow$	0.94	150	140
$e^\downarrow$	1.17	120	140
$h^\uparrow$	0.77	300	230

the energy and the momentum component parallel to the interface are conserved [15]. This allows us to calculate the normal-to-interface momentum component of the injected HCs and the corresponding  $v_{\text{Au}}^{\text{HC}}$ . The velocities were calculated based on density functional theory using band structures of bulk Au obtained within the Vienna Ab Initio simulation package (VASP) [23] with the projector augmented waves basis sets [24,25]. The energy-dependent  $\tau_{\text{Au}}^{\text{HC}}$  (Fig. 3) is reproduced from Ref. [26], where it was obtained as a fit to the results of time-resolved two-photon photoemission experiments. Although time-resolved two-photon photoemission is not sensitive to elastic scattering dominating the transport experiments [7], these results are still suitable for estimations due to low defect concentration in epitaxial Fe/Au structures studied here [15] vs polycrystalline films investigated in, e.g., Ref. [7].

The  $\tau_{\text{Au}}^{\text{HC}}$  and corresponding  $\lambda_{\text{Au}}^{\text{HC}}$  in Table I show that  $h^\downarrow$  and  $e^\downarrow$  give a moderate diffusive contribution to both  $\text{HC}^+$  and  $\text{HC}^-$  transport because  $\lambda_{\text{Au}}^{\text{HC}}$  is slightly larger than  $d_{\text{Au}}$ . In contrast, HCs generated in the majority Fe subband give an almost pure ballistic contribution to the  $\text{HC}^-$  ( $\lambda_{\text{Au}}^{h^\downarrow} \gg d_{\text{Au}}$ ) and an essentially diffusive one to the  $\text{HC}^+$  ( $\lambda_{\text{Au}}^{e^\downarrow} \leq d_{\text{Au}}$ ) transport supporting the above scenario. Since  $\tau_{\text{Au}}^S$  is independent of  $d_{\text{Au}}$ , it should be related to  $\tau_{\text{Au}}^{\text{HC}^+}$  only:  $\tau_{\text{Au}}^S = \tau_{\text{Au}}^{\text{HC}^+} / \eta_{\text{Au}}^{\text{SF}}$ , where  $\eta_{\text{Au}}^{\text{SF}}$  is the HC spin-flip probability for HC scattering at equilibrium carriers, phonons, or defects. Taking  $\tau_{\text{Au}}^{\text{HC}^+} \approx 100$  fs and  $\tau_{\text{Au}}^S \approx 1$  ps, we derive  $\eta_{\text{Au}}^{\text{SF}} \approx 0.1$ , which is a reasonable value [27]. Thus, our results (Fig. 2) can be indeed attributed to the competition between different contributions to the superdiffusive [6] transport of spin-polarized HCs, which are closer to either ballistic or diffusive limits depending on the HC spin orientation.

For applications, it could be rewarding to have a pure  $\text{HC}^-$  or  $\text{HC}^+$  contribution since it would represent a single-polarity SC pulse. In this regard, it is worth mentioning that excitation of samples with  $d_{\text{Fe}} = 3$  nm by an intense laser beam led to (i) a three time increase of the negative peak amplitude in  $\rho(t)$  and  $\Delta(t)$  and (ii) a reduction of the positive feature in  $\rho(t)$ . We attribute these effects to a laser-induced modification of the Fe/Au interface increasing the  $\text{HC}^-$  and reducing the  $\text{HC}^+$  fractions.

Therefore, controlled structural modifications might provide 100 fs single-polarity SC pulses. Estimations of SC density were made based on the absorbed pump fluence. We arrive at an SC on the order of  $10^8$ – $10^9$  A/cm<sup>2</sup> or  $10^{14}$ – $10^{15}$  HC/cm<sup>2</sup>/pulse or 0.1–1 HC/atom/pulse. In future experiments, one more ferromagnetic layer will be prepared on top of Au(001). Since the magnetization dynamics in such a magnetic top layer is triggered exclusively by spin-polarized HCs but not by a direct laser excitation or lattice heating, such experiments might help to unravel the origin of ultrafast magnetization dynamics.

In conclusion, a time-of-flight-like investigation of spin transport is demonstrated in Au/Fe/MgO(001). Spin current pulses formed by spin-polarized hot carriers excited in Fe are detected at the Au surface, and propagation velocities of different carrier contributions are analyzed. The duration of the spin current pulse is defined by the hot carrier spin relaxation time in Au, which was measured to be about 1 ps. The sign of the spin current changes within the overall pulse duration due to a competition of ballistically and diffusively propagating spin-polarized contributions, which are determined by energy-dependent scattering probabilities for the hot carriers initially excited in exchange-split bands of Fe.

Financial support by the DFG through ME 3570/1-1 and SFB 668 (TPA3) and partly by the Russian Foundation for Basic Research is gratefully acknowledged.

\*melnikov@fhi-berlin.mpg.de

†Present address: Radboud University, Nijmegen, The Netherlands.

‡Present address: Uppsala University, Sweden.

- [1] A. Kirilyuk, A. V. Kimel, and T. Rasing, *Rev. Mod. Phys.* **82**, 2731 (2010).
- [2] B. Koopmans *et al.*, *Phys. Rev. Lett.* **95**, 267207 (2005).
- [3] B. Koopmans *et al.*, *Nature Mater.* **9**, 259 (2010).
- [4] J.-Y. Bigot, M. Vomir, and E. Beaurepaire, *Nature Phys.* **5**, 515 (2009).
- [5] G. P. Zhang *et al.*, *Nature Phys.* **5**, 499 (2009).
- [6] M. Battiato, K. Carva, and P.M. Oppeneer, *Phys. Rev. Lett.* **105**, 027203 (2010).
- [7] R. Jansen, *J. Phys. D* **36**, R289 (2003).
- [8] G. Malinowski *et al.*, *Nature Phys.* **4**, 855 (2008).
- [9] S.D. Brorson, J.G. Fujimoto, and E.P. Ippen, *Phys. Rev. Lett.* **59**, 1962 (1987).
- [10] T. Juhasz *et al.*, *Phys. Rev. B* **48**, 15488 (1993).
- [11] A. Borisov *et al.*, *Chem. Phys. Lett.* **387**, 95 (2004).
- [12] D.C. Ralph and M.D. Stiles, *J. Magn. Magn. Mater.* **320**, 1190 (2008).
- [13] T. Mühge *et al.*, *Appl. Phys. A* **59**, 659 (1994).
- [14] D.T. Dekadjevi *et al.*, *Phys. Rev. Lett.* **86**, 5787 (2001).
- [15] The epitaxial growth is essential to obtain a well-defined structure suitable for *ab initio* analysis and minimize the diffusive contribution to the HC transport originating from the scattering on lattice inhomogeneities [10].

- [16] R.-P. Pan, H.D. Wei, and Y.R. Shen, *Phys. Rev. B* **39**, 1229 (1989).
- [17] J. Wang, B.-F. Zhu, and R.-B. Liu, *Phys. Rev. Lett.* **104**, 256601 (2010).
- [18] L. K. Werake and H. Zhao, *Nature Phys.* **6**, 875 (2010).
- [19] C. Suárez, W. E. Bron, and T. Juhasz, *Phys. Rev. Lett.* **75**, 4536 (1995).
- [20] A. Y. Elezzabi, M.R. Freeman, and M. Johnson, *Phys. Rev. Lett.* **77**, 3220 (1996).
- [21] P. Blaha *et al.*, *WIEN2K, An Augmented Plane Wave + Local Orbitals Program for Calculating Crystal Properties* (Vienna University of Technology, Austria, 2001).
- [22] J. P. Perdew, K. Burke, and M. Ernzerhof, *Phys. Rev. Lett.* **77**, 3865 (1996).
- [23] G. Kresse and J. Hafner, *J. Phys. Condens. Matter* **6**, 8245 (1994).
- [24] P. E. Blöchl, *Phys. Rev. B* **50**, 17953 (1994).
- [25] G. Kresse and D. Joubert, *Phys. Rev. B* **59**, 1758 (1999).
- [26] J. Cao *et al.*, *Phys. Rev. B* **58**, 10948 (1998).
- [27] C.L. S. Kantner *et al.*, *Phys. Rev. B* **83**, 134432 (2011).